Structure and stability of aluminium doped lithium clusters (Li nAl0/+, n = 1–8): A case of the phenomenological shell model

ARTICLE *in* PHYSICAL CHEMISTRY CHEMICAL PHYSICS · OCTOBER 2010

Impact Factor: 4.49 · DOI: 10.1039/c003401k · Source: PubMed

3 AUTHORS, INCLUDING:

Truong Tai
University of Leuven
67 PUBLICATIONS **524** CITATIONS
SEE PROFILE

Minh Tho Nguyen
University of Leuven
750 PUBLICATIONS **11,210** CITATIONS
SEE PROFILE

Structure and stability of aluminium doped lithium clusters ($Li_nAl^{0/+}$, n = 1–8): a case of the phenomenological shell model†

Truong Ba Tai,[a] Pham Vu Nhat[a] and Minh Tho Nguyen*[ab]

Received 22nd February 2010, Accepted 9th June 2010
DOI: 10.1039/c003401k

Quantum chemical calculations are performed on the aluminium doped lithium clusters Li_nAl at both neutral and cationic states using the DFT/B3LYP and CCSD(T) methods in conjugation with the aug-cc-pV*a*Z (a = D,T,Q) basis sets. The global minima are located and the growth mechanism is established. The electronic structure, geometrical parameters and energetic properties, such as average binding energy E_b, second difference of energy Δ^2E, adiabatic and vertical ionization energy, and dissociated enthalpy, are evaluated using the coupled-cluster CCSD(T) method, whose energies are extrapolated to the complete basis set limit (CBS). The high stability of Li_5Al, Li_7Al, Li_6Al^+ and Li_8Al^+ that have the "magic numbers" of valence electrons, can be understood using the phenomenological shell model.

Introduction

Clusters of the elements continue to attract the attention of scientists, experimental and theoretical alike, in part due to the fact that they are genuine intermediates between the atoms and bulk materials. The electronic structure, and thereby physical and chemical properties, of the clusters can be significantly different from not only those of bulk materials, but also from each other, depending on their actual size. One of the advantages of quantum chemical studies of small clusters is that they can be treated on the same footing as gas phase species by the same methods. However, similar to the situation in other fields, it is not always straightforward to understand the calculated results, which often need to be interpreted with the help of some simpler theoretical models. In this regard, the phenomenological shell model (PSM) which was proposed by Knight and co-workers in 1984[1] has been proven to be a simple but effective model to interpret the stability pattern and electronic structure of simple metal clusters.[2–4] Similar to the spherical jellium model (SJM),[5] the PSM valence electrons are assumed to be freely itinerant in a simple mean-field potential that is formed by the nuclei of atoms. A fundamental difference between the SJM and PSM is that while the many-body problem of the valence electrons in the SJM is treated self-consistently by quantum chemical methods, the PSM considers only the possible states of a single electron confined in a potential well of a given shape.[6] Accordingly, the high stability of a metal cluster is achieved if its electronic shell or sub-shells are closed, and the number of valence electrons corresponds to a shell closing, such as 2 ($1S^2$), 8 ($1S^2$ $1P^6$), 20 ($1S^2$ $1P^6$ $1D^{10}$ $2S^2$), *etc.*, which are called the "magic numbers". However, it is known that the simple PSM is not consistent with some highly stable binary clusters whose number of valence electrons does not correspond to these magic numbers, such as the case of K_8Zn[7] and Na_6Pb[8]. A modified (Wood-Saxon) potential was subsequently introduced as an extended model to account for the behavior of these cases.[9,10] According to this modified model, the dopant induces a perturbation and the ordering of the single particle energy levels is changed either to ($1S^2$ $1P^6$ $2S^2$ $1D^{10}$ $2P^6$) if the impurity is more electronegative than the host atoms, or to ($1S^2$ $1P^6$ $1D^{10}$ $2S^2$ $1F^{16}$ $2P^6$) if the central dopant is less electronegative than the host atoms. In this context, a legitimate question is whether the PSM can be applied to the binary clusters that include alkali metals. To tackle this question, we set out to perform a systematic investigation of the aluminium doped lithium clusters Li_nAl (n = 1–8) in both neutral and cationic states.

The aluminium-lithium clusters have received much attention. Cheng *et al.*[11] investigated the energetics and structures of Li_nAl (n = 1–8) and $AlLi_{17}$ using a local spin density functional method in conjunction with nonlocal pseudo-potentials. These authors found that Li_5Al is an especially stable species and plays the role of a building block for the Li_nAl clusters. Motivated by this idea, larger binary systems with the number of Al atoms up to eleven, such as $Li_{10}Al_n$ (n = 1 and 2),[12] $Li_{10}Al_8$,[13] Al_NLi_N (N = 1–6, 10),[14] and Al_nLi_n (n = 1–11),[15] were extensively studied. However, most previous reports focused on the geometrical structures and energetic properties of clusters, whereas the electronic structures that play an important role for the stability and properties of clusters were not fully understood. In addition, the lack of vibrational analyses of the structures led to the fact that the location of the global minima was not properly performed. Moreover, according to our best knowledge, no earlier theoretical investigation is available on the cationic clusters Li_nAl^+. In the present work, we search for the global minima of the clusters $Li_nAl^{0/+}$, and probe the growth mechanism of the neutral Li_nAl. The stability pattern of these clusters is further interpreted using the phenomenological shell model (PSM).

[a] *Department of Chemistry, and LMCC-Mathematical Modeling and Computational Science Center, Katholieke Universiteit Leuven, B-3001 Leuven, Belgium. E-mail: minh.nguyen@chem.kuleuven.be*
[b] *Institute for Computational Science and Technology of HoChiMinh City, Thu Duc, HoChiMinh City, Vietnam*

† Electronic supplementary information (ESI) available: Tables list the total electronic energies, zero-point energies and Cartesian coordinates of the structures considered. Figures display the molecular orbitals. See DOI: 10.1039/c003401k

Computational methods

All electronic structure calculations are carried out using the Gaussian 03[16] and Molpro 2008[17] program packages. Equilibrium geometries and harmonic vibrational frequencies of clusters are fully investigated using density functional theory with the hybrid functional B3LYP,[18–20] in conjunction with the correlation consistent aug-cc-pVTZ basis set. To obtain more accurate results, the geometries, vibrational frequencies and energies of the lowest-lying isomers are subsequently refined using the restricted/unrestricted coupled-cluster theory formalism (R/UCCSD(T))[21–24] with

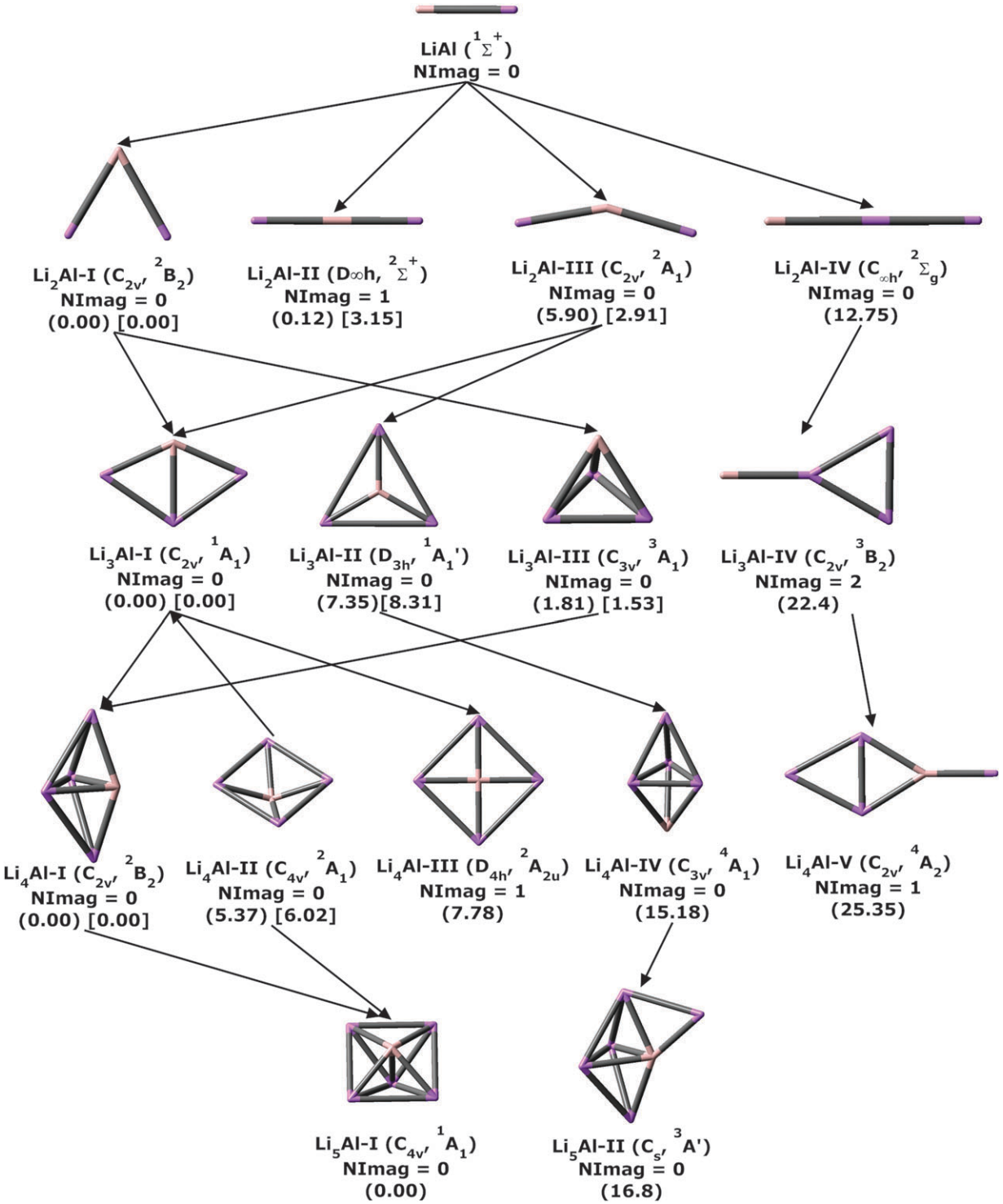

Fig. 1 Shape of the optimized structures for the neutral Li_nAl (n = 1–5). Relative energies (ΔE, kcal mol^{-1}) are obtained from B3LYP/aug-cc-pVTZ (in parentheses) and CCSD(T)/aug-cc-pVTZ (in brackets) calculations. All values are corrected for ZPEs. NImag stands for the number of imaginary frequencies.

the aug-cc-pV*a*Z (*a* = D,T,Q) basis sets. The coupled-cluster energies are then extrapolated to the complete basis set (CBS). The procedures for evaluating these energies are given in detail in recent papers.[25–27] The natural bond orbitals (NBO)[28–30] are constructed using B3LYP/6-311+G(d) densities. An analysis of the electron localizability indicator (ELI-D)[31] is also performed to understand the nature of chemical bonding. Similar to the electron localization function (ELF), the ELI-D and its orbital decomposition[32] are proven to be an effective tool to study the chemical bonding in organic compounds as well as in transition metal compounds.[33] The ELI-D is defined as the integral of the electron density over micro-cell containing the same fraction of same-spin electron pairs. It can be considered to be a product of the pair volume function and the electron density, and is a sum of orbital densities in the case of single determinant wave functions. Thus, ELI-D can be decomposed into molecular orbital contributions that are called the partial electron localizability indicator (pELI).[32] The ELI-D values are calculated using the DGrid-4.2 program suite[34] and the ELI isosurfaces are plotted using the Gopenmol software.[35]

Results and discussion

Global minima and growth mechanism of the neutral Li_nAl

In this section, we mainly focus on the neutral clusters Li_nAl with *n* ranging from 1 to 8. The structural shape of the lower-lying isomers, together their relative energy (kcal mol^{-1}) and the associated number of imaginary frequencies are depicted in Fig. 1 and 2. As for a necessary calibration, geometrical parameters, total energies and vertical ionization energies (vIE) of the small clusters, *n* = 1–5, are obtained using CCSD(T) calculations, in conjugation with the aug-cc-pV*a*Z, with *a* = D,T,Q. The electronic energies are subsequently extrapolated to the complete basis set limits.[36] The calculated results are presented in Table 1. It turns out that while the CCSD(T)/aug-cc-pVDZ values are rather unsatisfactory, there are small differences between the calculated results using the aug-cc-pVTZ, and aug-cc-pVQZ basis sets, with respect to the CBS values. The vIEs determined using these basis sets vary only in the range of 0.01–0.04 eV. Therefore, for the larger clusters, Li_nAl (*n* = 6–8), the calculations are performed using only the CCSD(T)/aug-cc-pVTZ levels, due to the limitation of our computational resources.

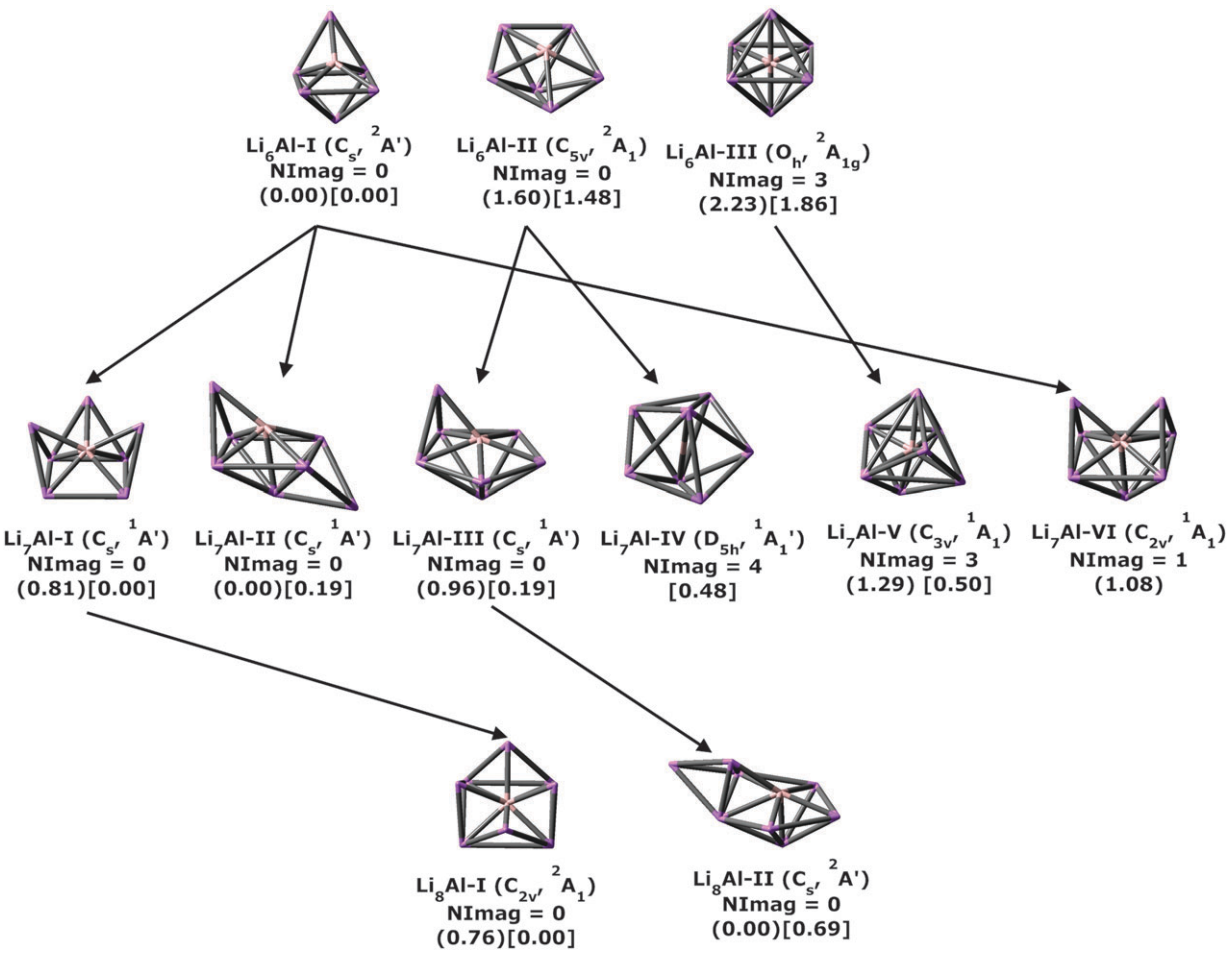

Fig. 2 Shape of the optimized structures for the neutral Li_nAl (*n* = 6–8). Relative energies (ΔE, kcal mol^{-1}) are obtained from B3LYP/aug-cc-pVTZ (in parentheses) and CCSD(T)/aug-cc-pVTZ (in brackets) calculations. All values are corrected for ZPEs. NImag stands for the number of imaginary frequencies.

Table 1 Geometrical parameters and vertical ionization energies (vIEs) of small clusters Li_nAl (n = 1–5) using the CCSD(T)/aug-cc-pVaZ (a = D, T, Q) levels of theory

Methods	$r_{Al–Li}$/Å	$r_{Al–Li'}$/Å	(Li–Al–Li) (degree)	vIEs/eV
LiAl ($^1\Sigma^+$)				
CCSD(T)/aug-cc-pVDZ	2.886	—	—	5.14
CCSD(T)/aug-cc-pVTZ	2.898	—	—	5.21
CCSD(T)/aug-cc-pVQZ	2.866	—	—	5.23
CCSD(T)/CBS	—	—	—	5.25
Li_2Al (C_{2v}, $^2B_2$)				
CCSD(T)/aug-cc-pVDZ	2.555	—	75.5	5.83
CCSD(T)/aug-cc-pVTZ	2.898	—	60.0	5.23
CCSD(T)/aug-cc-pVQZ	2.860	—	60.4	5.27
CCSD(T)/CBS	—	—	—	5.31
Li_3Al (C_{2v}, $^1A_1$)				
CCSD(T)/aug-cc-pVDZ	2.696	2.838	133.8	5.19
CCSD(T)/aug-cc-pVTZ	2.761	2.904	131.4	5.20
CCSD(T)/aug-cc-pVQZ	2.722	2.851	133.7	5.23
CCSD(T)/CBS	—	—	—	5.25
Li_4Al (C_{2v}, $^2B_2$)				
CCSD(T)/aug-cc-pVDZ	2.662	2.699	62.2	5.01
CCSD(T)/aug-cc-pVTZ	2.785	2.727	62.1	4.93
CCSD(T)/aug-cc-pVQZ	2.743	2.692	62.1	4.96
CCSD(T)/CBS	—	—	—	4.98
Li_5Al (C_{4v}, $^1A_1$)				
CCSD(T)/aug-cc-pVDZ	2.596	2.766	130.9	5.06
CCSD(T)/aug-cc-pVTZ	2.662	2.873	129.9	5.03
CCSD(T)/aug-cc-pVQZ	2.638	2.818	130.7	5.02
CCSD(T)/CBS	—	—	—	5.02

The diatomic LiAl has a low spin ground state ($^1\Sigma^+$) (Fig. 1) with singlet–triplet separation gap of −5.0 kcal mol^{-1}. Adding one Li atom to LiAl, four stationary structures are obtained for Li_2Al, including a bent form **Li_2Al-I** (C_{2v}, $^2B_2$), a linear saddle-point **Li_2Al-II**, and a slightly bent **Li_2Al-III** (C_{2v}, $^2A_1$), and a linear structure **Li_2Al-IV** with a LiLiAl connectivity. The structure **Li_2Al-I**, whose SOMO is a bonding σ-orbital (b_2), is the most stable isomer, whereas its counterpart **Li_2Al-III** (C_{2v}, $^2A_1$), whose SOMO is a non-bonding orbital mainly composed of 3p-orbital of Al, is found to be the first excited state with an energy gap of 2.9 kcal mol^{-1} (CCSD(T)/aug-cc-pVTZ). The linear **Li_2Al-II** is a transition structure that is 3.2 kcal mol^{-1} above **Li_2Al-I**.

Binding one additional Li atom to the Al atom of the global minimum, **Li_2Al-I**, gives rise to three Li_3Al structures, including the planar **Li_3Al-I** (C_{2v}), the high symmetry **Li_3Al-II**(D_{3h}) and the three-dimensional form **Li_3Al-III**(C_{3v}) in which the Al atom was located on the C_3 axis of the triangular Li_3. In an earlier report, Cheng *et al.*[11] showed that the high spin **Li_3Al-III** (C_{3v}, $^3A_1'$) is the most stable isomer for the neutral Li_3Al. At the high accuracy CCSD(T) method, we find that the low spin **Li_3Al-I** (C_{2v}, $^1A_1$) is the global minimum, being 1.5 kcal mol^{-1} more stable than the high spin **Li_3Al-III** (C_{3v}, $^3A_1'$). The singlet **Li_3Al-II** (D_{3h}, $^1A_1'$) is also a stable isomer, being 7.3 kcal mol^{-1} less table than the first. A question arises as to why the perfect triangle **Li_3Al-II** is less stable than the **Li_3Al-I**. In **Li_3Al-II**, the Al center has the valence orbital occupation of Al $2s^{0.33}$ $2p^{0.67}$ which corresponds to a sp^2 hybridization. Consequently, chemical bonds that are formed by overlap of these hybridized orbitals and s-orbital of Li atoms, are located mainly on the Al center. The natural charge populations reveal a high ionic character of **Li_3Al-II**, with a strongly negative net charge on Al (q(Al) = −1.7 electron), whereas more covalent character is found in **Li_3Al-I** (q(Al) = −1.05, q($Li_{1,2}$) = 0.45 and q(Li_3) = 0.14 electron). Thus the singlet **Li_3Al-I** can be considered as a combination of a triangle Li_2Al and Li atom. The form **Li_3Al-IV** is a second-order saddle-point.

It is remarkable to note that the appearance of the first 3D global minimum in the series of Li_nAl is already found for Li_4Al. Various structures for Li_4Al are constructed by binding one Li atom to the low-lying Li_3Al isomers. A high symmetry planar form, **Li_4Al-III** (D_{4h}, $^2A_{2u}$), turns out to be a transition structure for a Jahn–Teller effect. Consequently, two lower symmetry forms, **Li_4Al-I** (C_{2v}, $^2B_2$) and **Li_4Al-II** (C_{4v}, $^2A_1$), are obtained as equilibrium structures. At the CCSD(T)/aug-cc-pVTZ level, **Li_4Al-I** is the global minimum, whereas **Li_4Al-II** is the next isomer with a relative energy of 6.0 kcal mol^{-1}. These predictions are also consistent with the PSM in that the system Li_4Al contains seven valence electrons, and its seventh valence electron singly occupies a P_z orbital in the shell of $1S^2$ $1P^5$ ($1P_x^2$ $1P_y^2$ $1P_z^1$). Consequently, the global minimum of the Li_4Al possesses a 3D structure. Other stationary structures are also located and displayed in Fig. 1.

In agreement with an earlier report,[11] the structure **Li_5Al-I** (C_{4v}, $^1A_1$), in which the 5th Li atom connects directly with Al of **Li_4Al-II**, is the most stable isomer of the six-atom system. The high spin **Li_5Al-II** (C_s, $^3A'$) is the second lowest-lying isomer, being 16.8 kcal mol^{-1} higher in energy. Various structures are equally constructed for Li_5Al but their geometries are invariably converged to the C_{4v} structure and no other structure can thus be located.

The lower-lying isomers and also the growth mechanism for the larger clusters, Li_nAl with n = 6–8, are examined and the results are summarized in Fig. 2. The high symmetry structure **Li_6Al-III** (O_h, $^2A_{2g}$) is found to be a high-order saddle point with three imaginary frequencies. The low symmetry **Li_6Al-I** (C_s, $^2A'$), which is distorted from the higher symmetry O_h form, and the doublet **Li_6Al-II** (C_{5v}, $^2A_1$) are close in energy with a small difference of 1.5 kcal mol^{-1}.

Various Li_7Al structures are constructed by binding one excess Li atom to the low-lying isomers Li_6Al at different positions (Fig. 2). Three low-energy structures are located, including (i) **Li_7Al-I** (C_s) in which Li is connected directly with Al of the neutral **Li_6Al-I**, (ii) **Li_7Al-II** in which a Li is absorbed on a Li_3 surface of the **Li_6Al-I**, and (iii) **Li_7Al-III** where one Li simply binds to Al of **Li_6Al-II**. According to our CCSD(T)/aug-cc-pVTZ results, these structures are quasi-degenerate with a similar energy content. High symmetry structures such as **Li_7Al-IV** (D_{5h}), **Li_7Al–V** (C_{3v}) and **Li_7Al-VI** (C_{2v}) turn out to be saddle points, with each having at least one imaginary frequency.

The addition of one excess Li atom to the lower-lying Li_7Al isomers gives rise to two degenerate structures for the neutral Li_8Al, including **Li_8Al-I** (C_{2v}), in which Al possesses an eight coordination state, and **Li_8Al-II** (C_s), in which Al has seven coordinates. Our calculated results show that both structures are practically degenerate.

In summary, the small clusters Li_nAl (n = 1–8) considered tend to be constructed by binding the additional lithium atom to the lowest-lying isomer of the smaller system $Li_{n-1}Al$. The growth motif dominantly prefers to increase the coordination state of the Al impurity when the number of Li atoms is $n \leq 6$. Compared to the similar system Li_nB (n = 1–8),[37] the global minima of the Li_nAl clusters tend to be more opened. While the boron impurity of the Li_nB system usually occupies a central position in lithium cage giving high symmetry structures, such as Li_3B (D_{3h}), Li_4B (D_{2d}), Li_6B (O_h), Li_7B (D_{5h}) and Li_8B (C_{3v}), the aluminium impurity appears to favor the opened structures, which can be understood by the larger size of Al, as compared to that of B. The Li_nAl also show many differences in terms of structures as compared with the Li_nGe systems that have been detected experimentally by using mass spectrometric techniques.[38]

The global minima of the cationic clusters Li_nAl^+ (n = 1–8)

Cationic structures Li_nAl^+ are generated from the located neutral Li_nAl structures, and the obtained geometries are summarized in Fig. 3.

Following detachment of one electron from the HOMO of LiAl ($^1\Sigma^+$), the low spin $LiAl^+$ ($^2\Sigma^+$) becomes the global minimum of the diatomic ion. Although the structure **Li_2Al-IIc** (C_{2v}, $^1A_1$) is still located as a local minimum, the linear **Li_2Al-Ic** ($^1\Sigma_g^+$) becomes the global minimum for Li_2Al^+, with a relative energy of 17.3 kcal mol^{-1} (B3LYP/aug-cc-pVTZ). For Li_3Al^+, the doublet **Li_3Al-Ic** (C_{2v}, $^2B_2$), which is a distorted form of the vertical ion of **Li_3Al-II** (D_{3h}) under a Jahn–Teller effect, is the lowest-lying isomer. Its distorted counterpart **Li_3Al-IIc** (C_{2v}, $^2A_1$) is a transition structure with one imaginary frequency.

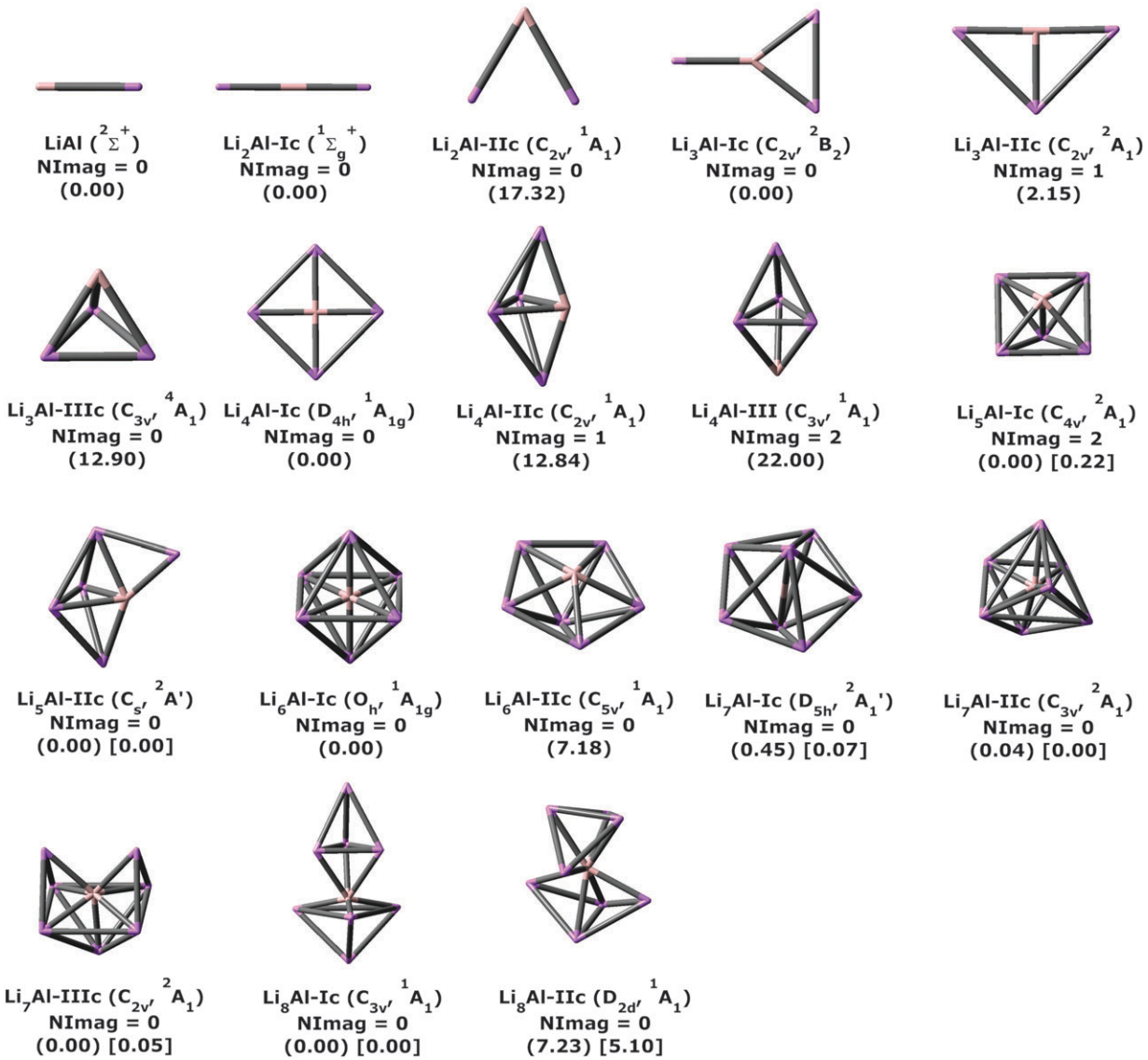

Fig. 3 Shape of the optimized structures for the cationic clusters Li_nAl^+ (n = 1–8). Relative energies (ΔE, kcal mol^{-1}) are from B3LYP/aug-cc-pVTZ (in parentheses) and CCSD(T)/aug-cc-pVTZ (in brackets) calculations. All values are corrected for ZPEs. NImag stands for the number of imaginary frequencies.

It is interesting to note that while the global minimum **Li_4Al-I** (C_{2v}, $^2B_2$) possesses the 3D structure, its cationic state prefers a planar shape, **Li_4Al-Ic** (D_{4h}, $^1A_{1g}$). This is consistent with the PSM that the six valence electrons of Li_4Al^+ fully occupied three valence orbitals of the PSM ($1S^2\ 1P_x^2\ 1P_y^2$), and thereby close the electron shells.

Removal of one electron from the degenerate HOMO of **Li_5Al-I** leads to a geometrical distortion under a Jahn–Teller effect. Consequently, the low symmetry structure **Li_5Al-IIc** (C_s, $^2A'$) is found to be the ion global minimum, while the distorted counterpart **Li_5Al-Ic** (C_{4v}, $^2A_1$) is now a second-order saddle-point (with two imaginary frequencies). According to the PSM, the cationic cluster Li_6Al^+, which contains eight valence electrons, is expected to be a highly stable species. Our calculated results show, in fact, that the global minimum of Li_6Al^+ has a perfect octahedral structure, **Li_6Al-Ic** (O_h, $^1A_{1g}$) (Fig. 3). The adiabatic ionization energy (IE) of Li_6Al obtained from energy difference between the neutral **Li_6Al-I** (C_s, $^2A'$) and the cation **Li_6Al-Ic** (O_h, $^1A_{1g}$) amounts to 3.59 eV, which represents the smallest value as compared to those obtained for the remaining examined members of the series Li_nAl. Additionally, its HOMO–LUMO energy gap of 2.45 eV corresponds to the highest value. Thus, these results support the view that this cation is a highly stable system.

There is a competition in the growth motif for the larger cationic clusters, Li_nAl^+ with $n = 7$ and 8. Firstly, the additional Li atom binds directly to Al of the $Li_{n-1}Al^+$ and thereby forms spherical-like structures, such as **Li_7Al-Ic**, **Li_7Al-IIIc**, and **Li_8Al-IIIc**. The second motif is a Li absorption on a (Li–Li–Li) face to make oblate structures such as **Li_7Al-IIc** and **Li_8Al-Ic**. According to our calculated results, the three structures **Li_7Al-Ic**, **Li_7Al-IIc** and **Li_7Al-IIIc** are energetically quasi-degenerate, and become the lowest-lying isomers of the Li_7Al^+ (Fig. 3). For Li_8Al^+, both structures **Li_8Al-Ic** and **Li_8Al-IIc** are also almost degenerate, and are $\sim$5 kcal mol^{-1} more stable than the singlet **Li_8Al-IIIc**.

Energetic properties

The relative stabilities of the clusters Li_nAl in both neutral and cationic states are examined on the basis of the average binding energy (E_b) and the second order difference in the total energies (Δ^2E) which are defined as follows:

$$E_b\ (Li_nAl) = [nE(Li) + E(Al) - E(Li_nAl)]/(n + 1) \quad (1)$$

$$E_b\ (Li_nAl^+) = [(n - 1)E(Li) + E(Li^+) + E(Al) - E(Li_nAl)]/(n + 1) \quad (2)$$

$$\Delta^2E(Li_nAl) = E(Li_{n-1}Al) + E(Li_{n+1}Al) - 2E(Li_nAl) \quad (3)$$

$$\Delta^2E(Li_nAl^+) = E(Li_{n-1}Al^+) + E(Li_{n+1}Al^+) - 2E(Li_nAl^+) \quad (4)$$

The second order difference in total energy, Δ^2E, of the Li_nAl is calculated as energy difference between two dissociation processes, namely, $Li_{n+1}Al \rightarrow Li_nAl + Li$ and $Li_nAl \rightarrow Li_{n-1}Al + Li$. Consequently, it reflects the relative stability of Li_nAl as compared to that of its two immediate neighbors, $Li_{n+1}Al$ and $Li_{n-1}Al$. A high value of Δ^2E indicates that this species has a high relative stability. The average binding energies, E_b, and the second order differences, Δ^2E, of the clusters considered are schematically illustrated in Fig. 4 and 5, respectively. It is observed that the average binding energy, E_b, in both two states considered increases with an increasing size of lithium number, and forms peaks at the neutral Li_5Al and the cation Li_6Al^+. Then they have a tendency to decrease somewhat when the number of Li atoms increases up to eight.

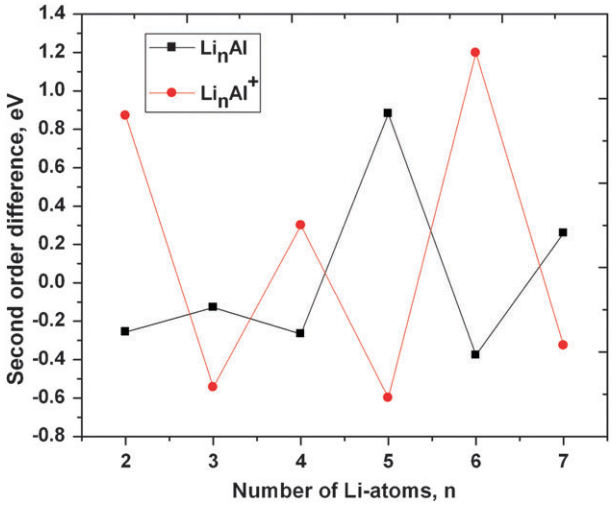

Fig. 4 Second difference in energy of the Li_nAl clusters (n = 1–8) at both neutral and cationic states using the CCSD(T)/aug-cc-pVTZ values.

As expected, an odd-even oscillation is found for the plots of the second order difference of clusters Li_nAl (Fig. 4). Consistent with the results of the average binding energy, the remarkably high values that were observed for the Li_5Al and the Li_6Al^+ emphasize their higher stability with respect to the remaining species.

HOMO–LUMO gaps and ionization energies (IEs)

The HOMO–LUMO gaps and ionization energies can also be regarded as measures of stability. A large gap suggests a relatively high stability, whereas a small IE reveals that the

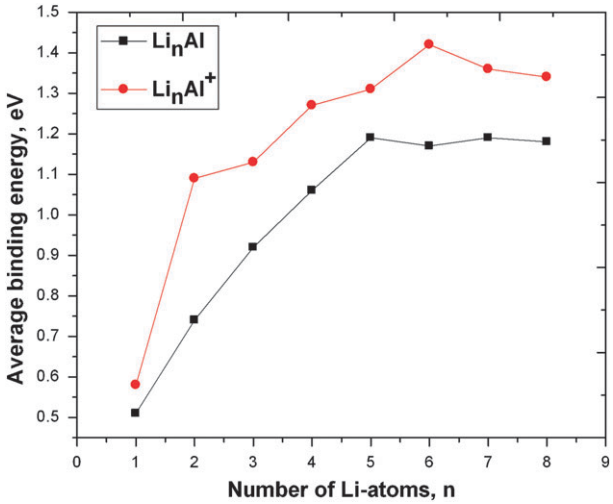

Fig. 5 Average binding energy of the Li_nAl clusters (n = 1–8) at both neutral and cationic states using the CCSD(T)/aug-cc-pVTZ values.

Table 2 The HOMO–LUMO (SOMO–LUMO for open-shell species) gaps (eV) of the $Li_nAl^{0/+}$ calculated at the B3LYP/6-311+G(d) level

Neutrals	HOMO–LUMO gap/eV	Cations	HOMO–LUMO gap/eV
LiAl ($^1\Sigma^+$)	1.62	LiAl ($^2\Sigma^+$)	2.24
Li_2Al-I (C_{2v}, $^2B_2$)	1.73	**Li_2Al-IIc** ($^1\Sigma^+$)	2.34
Li_3Al-I (C_{2v}, $^1A_1$)	1.69	**Li_3Al-Ic** (C_{2v}, $^2B_2$)	1.93
Li_4Al-I (C_{2v}, $^2A_1$)	1.56	**Li_4Al-IIIc** (D_{4h}, $^1A_1'$)	2.11
Li_5Al-I (C_{4v}, $^1A_1$)	2.03	**Li_5Al-IIc** (C_s, $^2A'$)	1.71
Li_6Al-I (C_1, ^2A)	1.00	**Li_6Al-IIIc** (O_h, $^1A_{1g}$)	2.45
Li_7Al-I (C_s, $^1A'$)	1.23	**Li_7Al-IVc** (C_{3v}, $^2A_1$)	1.04
Li_8Al-I (C_{2v}, $^2A_1$)	1.02	**Li_8Al-IIIc** (C_{3v}, $^1A_1$)	1.90

Table 3 The adiabatic (IEs) and vertical ionization (vIE) energies (eV) of Li_nAl (n = 1–8) using the CCSD(T)/aug-cc-pVTZ (CBS) levels of theory

Reactions	IE/eV	Reactions	vIE/eV
LiAl ($^1\Sigma^+$) − 1e → LiAl ($^2\Sigma^+$)	5.19 (5.23)[a]	LiAl ($^1\Sigma^+$) − 1e → LiAl ($^2\Sigma^+$)	5.21
Li_2Al-I (C_{2v}, $^2B_2$) − 1e → **Li_2Al-Ic** ($^1\Sigma^+$)	4.30 (4.29)	**Li_2Al-I** (C_{2v}, $^2B_2$) − 1e → Li_2Al (C_{2v}, $^1A_1$)	5.23
Li_3Al-I (C_{2v}, $^1A_1$) − 1e → **Li_3Al-Ic** (C_{2v}, $^2B_2$)	4.51 (4.52)	**Li_3Al-I** (C_{2v}, $^1A_1$) − 1e → Li_3Al (C_{2v}, $^2B_2$)	5.20
Li_4Al-I (C_{2v}, $^2A_1$) − 1e → **Li_4Al-Ic** (D_{4h}, $^1A_{1g}$)	4.27 (4.28)	**Li_4Al-I** (C_{2v}, $^2A_1$) − 1e → Li_4Al (C_{2v}, $^1A_1$)	5.20
Li_5Al-I (C_{4v}, $^1A_1$) − 1e → **Li_5Al-IIc** (C_s, $^2A'$)	4.63 (4.66)	**Li_5Al-I** (C_{4v}, $^1A_1$) − 1e → Li_5Al (C_{4v}, $^2A_1$)	5.03
Li_6Al-I (C_1, ^2A) − 1e → **Li_6Al-Ic** (O_h, $^1A_{1g}$)	3.59	**Li_6Al-I** (C_1, ^2A) − 1e → **Li_6Al** (C_1, ^1A)	3.87
Li_7Al-I (C_s, $^1A'$) − 1e → **Li_7Al-IIc** (C_{3v}, $^2A_1$)	3.96	**Li_7Al-I** (C_s, $^1A'$) − 1e → **Li_7Al** (C_s, $^2A'$)	4.83
Li_8Al-I (C_{2v}, $^2A_1$) − 1e → **Li_8Al-Ic** (C_{3v}, $^1A_1$)	3.61	**Li_8Al-I** (C_{2v}, $^2A_1$) − 1e → **Li_8Al** (C_{2v}, $^1A_1$)	3.90

[a] Values given in parentheses are obtained using the extrapolated CCSD(T)/CBS energies.

corresponding cation is a more stable isomer. The frontier orbital gaps of the neutral clusters Li_nAl (Table 2) show a remarkably large value at Li_5Al, while the largest value of Li_nAl^+ is found at Li_6Al^+.

There is a large difference between the adiabatic IE and vIE values (Table 3), which can be understood from the important geometry differences of the global minima in both neutral and cationic states. In addition, the systems where the shells are closed, such as Li_5Al, Li_7Al, show high IE values, whereas the Li_6Al and Li_8Al clusters are characterized by the smallest IEs. As a consequence, consistent with the results of Δ^2E, E_b and HOMO–LUMO gaps, the neutral Li_5Al and Li_7Al, and also the cations Li_6Al^+ and Li_8Al^+ are expected to exhibit high relative stability.

Dissociation energies

To probe further the thermodynamic stability of the clusters, we examine their dissociation energies. For the neutral clusters, the reaction energies for the channels:

$$Li_nAl \rightarrow Li_{n-1}Al + Li$$

$$Li_nAl \rightarrow Li_n + Al$$

$$Li_nAl \rightarrow Li_{n-2}Al + Li_2$$

are considered and the calculated results are summarized in Table 4. For the cationic clusters, Li_nAl^+, two dissociation channels:

$$Li_nAl^+ \rightarrow Li_{n-1}Al^+ + Li$$

$$Li_nAl^+ \rightarrow Li_{n-1}Al + Li^+$$

are examined and the results are tabulated in Table 5. From the plots of all channels in Fig. 6, it can be seen that decomposition of the neutral Li_nAl to give one Li atom plus one fragment $Li_{n-1}Al$ is endothermic by the smallest energy. Except for Li_2Al^+, the dissociation reaction of Li_nAl^+ giving one Li atom plus a radical $Li_{n-1}Al^+$ is consistently more favorable than that giving Li^+ plus the fragment $Li_{n-1}Al$. The neutral Li_5Al and the cation Li_6Al^+ emerge to have the largest values of dissociation energy as compared to their neighbors, which is consistent with their high stability detected above from other properties.

Table 4 Dissociation enthalpies (kcal mol^{-1}) of the clusters Li_nAl using the CCSD(T)/aug-cc-pVTZ+ZPE level

Neutral clusters	$Li_nAl \rightarrow Li_{n-1}Al + Li$	$Li_nAl \rightarrow Li_{n-2}Al + Li_2$
LiAl ($^1\Sigma^+$)	22.9	—
Li_2Al-I (C_{2v}, $^2B_2$)	27.3	26.9
Li_3Al-I (C_{2v}, $^1A_1$)	33.0	37.0
Li_4Al-I (C_{2v}, $^2A_1$)	35.8	45.4
Li_5Al-I (C_{4v}, $^1A_1$)	41.9	54.4
Li_6Al-I (C_1, ^2A)	24.0	42.6
Li_7Al-I (C_s, $^1A'$)	28.9	29.5
Li_8Al-I (C_{2v}, $^2A_1$)	24.7	30.3

Aromaticity and electron localizability indicator (ELI) of high stability structures

The concept of aromaticity is now extensively applied to metal clusters.[39] Aromatic metal clusters usually possess high symmetry structures and good electron delocalization. Alexandrova *et al.*[40] suggested that the pure lithium clusters Li_n (n = 5–7) are aromatic systems from an analysis of their molecular orbitals. The aromaticity of lithium and aluminium based complexes were recently examined by Pati and his co-workers.[41] Thus, a question arises as to whether the aluminium doped lithium clusters are also aromatic. The highly stable clusters Li_5Al, Li_6Al^+, Li_7Al and Li_8Al^+ turn out to possess high symmetry structures. We first perform an evaluation of aromaticity of these clusters by using the nucleus independent chemical shifts (NICS) index, which is based on

Table 5 Dissociation enthalpies (kcal mol^{-1}) of the cationic clusters Li_nAl^+ using the CCSD(T)/aug-cc-pVTZ + ZPE level

Cationic clusters	$Li_{n-1}Al^+ + Li$	$Li_{n-2}Al^+ + Li_2$	$Li_{n-1}Al + Li^+$	$Li_{n-2}Al + Li_2^+$
LiAl ($^2\Sigma^+$)	40.2	—	26.3	—
Li2Al-IIc ($^1\Sigma^+$)	48.0	65.0	51.4	45.2
Li3Al-Ic (C_{2v}, $^2B_2$)	28.1	52.8	52.2	50.4
Li4Al-IIIc (D_{4h}, $^1A_1'$)	41.2	46.0	60.4	64.3
Li5Al-IIc (C_s, $^2A'$)	33.7	51.6	58.4	65.1
Li6Al-IIIc (O_h, $^1A_{1g}$)	47.9	58.3	64.4	77.2
Li7Al-IVc (C_{3v}, $^2A_1$)	20.3	44.9	60.7	55.6
Li8Al-IIIc (C_{3v}, $^1A_1$)	33.0	29.9	64.8	64.6

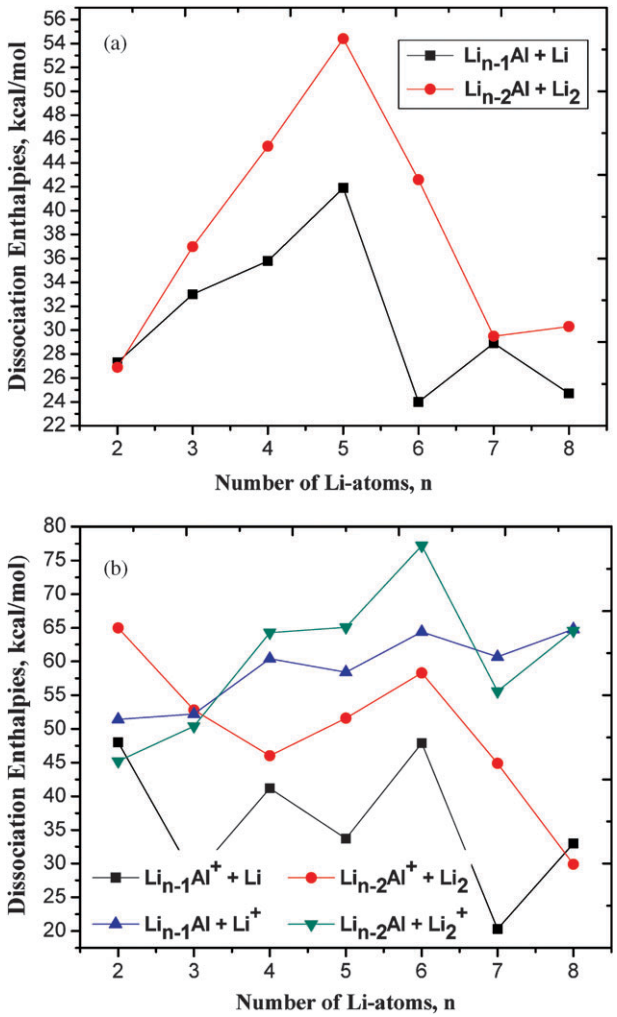

Fig. 6 Dissociation enthalpies of (a) the neutral Li_nAl, and (b) the cation Li_nAl^+ using the CCSD(T)/aug-cc-pVTZ level.

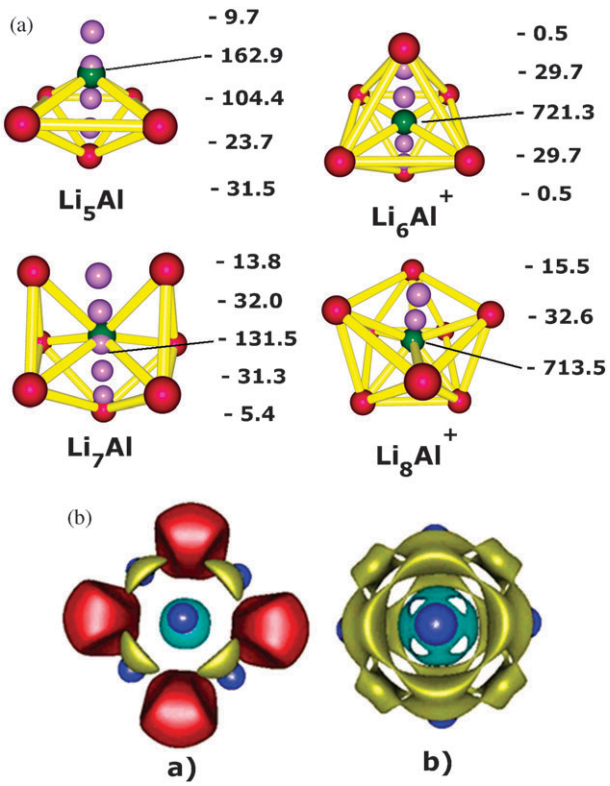

Fig. 7 (a) NICS values, and (b) pELI-D contributions for valence orbitals of the highly stable clusters.

magnetic shieldings.[42] The NICS values for the more stable clusters, Li_5Al, Li_6Al^+, Li_7Al and Li_8Al^+, are computed at various positions as shown in Fig. 7a. The distance between two evaluated positions is 1.0 Å. The calculated NICS values show that these species have an aromatic character with highly negative NICS values. Nevertheless, the very negative NICS values found around the position of Al is due to the effect of the impurity.

To further probe the chemical bonding and electron distribution, the electron localizability indicator (ELI) is used. The ELI plots for structures Li_5Al and Li_6Al^+ are depicted in Fig. 7b. The localization domains of Li and Al (in blue) are mainly composed of core orbitals. The isosurfaces of p-ELI distribution for the neutral Li_5Al reveal that the red-colored localization domains, that arise from p_x and p_y orbitals, are responsible for Li–Li bonding. The yellow-colored domain is composed of p_z orbital that is responsible for its aromaticity.

In a similar way, the p-ELI plots of the cation Li_6Al^+ point out that the yellow domains composed of three degenerate p-orbitals are distributed globally over the whole skeleton, which renders the system highly aromatic. In addition, there is an obvious presence of twelve localized basins distributed on Li–Li bonds of Li_6Al^+, which is in line with its high symmetry.

Phenomenological shell model (PSM)

To interpret the stability pattern, the PSM in which the Al impurity plays the role of an electronegative dopant is used. Because the impurity is more electronegative than the host, the

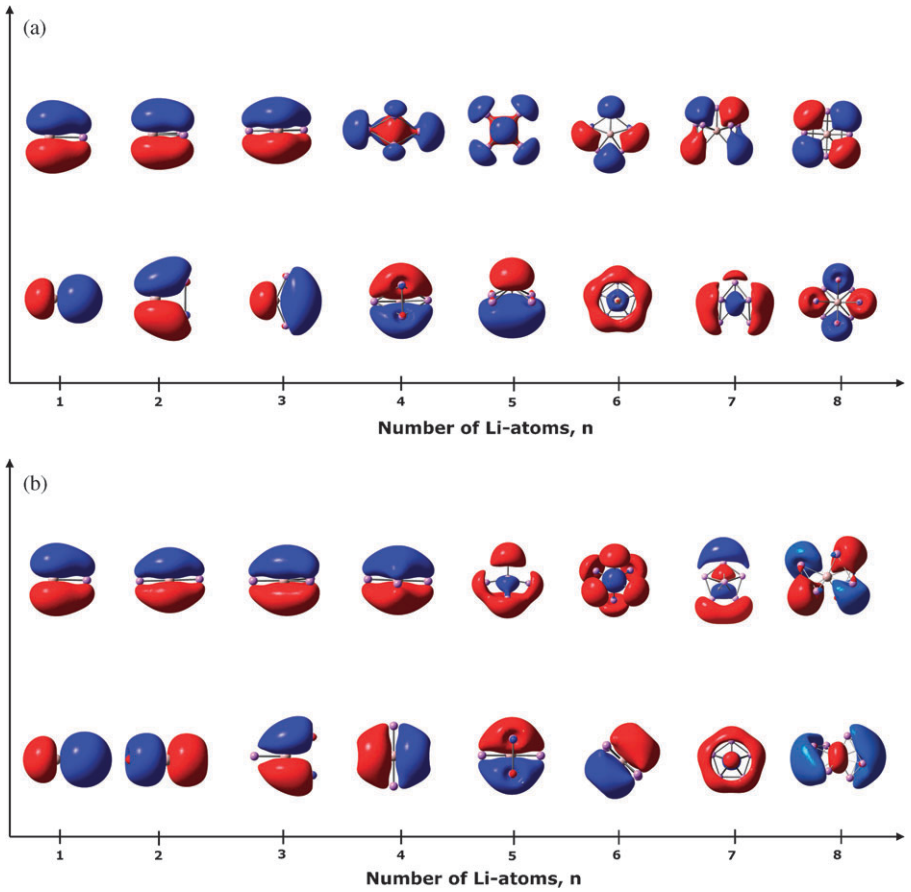

Fig. 8 HOMO and LUMO shapes of (a) the neutral clusters Li_nAl, and (b) the cationic clusters Li_nAl^+ (n = 1–8).

ordering of the single particle energy levels in the PSM is expected to be changed to the rearranged ordering of $1S^2\ 1P^6\ 2S^2\ 1D^{10}$.

The HOMO and LUMO shapes are shown in Fig. 8a (neutral clusters) and 8b (cations). First, the electronic shells of the neutral Li_nAl (n = 1–8) are consistent with the PSM description. The HOMO of small clusters Li_nAl with n = 1–5 has p-character, whereas the LUMO of Li_4Al and Li_5Al shows s-character, which agrees well with the energy level of $1S^2\ 1P^6\ 2S^2$ of the PSM. A similar interpretation can be put forward for the larger clusters in that the HOMOs of Li_7Al and Li_8Al are s-orbitals, while their LUMOs should be d-orbitals.

The PSM can also be applied to the charged species. In a similar way, Fig. 8b points out that the electronic shells of the cations Li_nAl^+ are very consistent with the ordering of energy levels of this model. The presence of quasi-degenerate structures for the larger size clusters, Li_nAl, n = 7 and 8, is an interesting case, which can be understood from a competition between two growth motifs: Li is either condensed directly with Al of the lower member $Li_{n-1}Al$ (**Li_7Al-Ic**, **Li_7Al-IIIc**, **Li_8Al-IIIc**) or adsorbed on a (Li–Li–Li) surface to form a lithium tetrahedral-like unit (**Li_7Al-IIc**, **Li_8Al-Ic**). While the first set bears spherical-like geometry and satisfies the PSM within the energy ordering of $1S^2\ 1P^6\ 2S^2\ 1D^{10}$, the second set shows other energy levels of $1S^2\ 1P^6\ 1D^2$, which can be interpreted by using the Clemenger-Nilsson model.[43] Both the neutral Li_5Al and cation Li_6Al^+ each contain eight valence electrons, which is the magic number for the electronic shell of $1S^2\ 1P^6$. Accordingly, these clusters constitute the highly stable members of the series examined.

Conclusion

We carried out a systematic investigation on the aluminium doped lithium clusters Li_nAl (n = 1–8) in both neutral and cationic states using the DFT and CCSD(T) methods. Their global energy minima are found or confirmed, and their electronic structure is examined in detail. A growth mechanism of the clusters can be formulated as follows: (i) the small clusters with n = 1–6 tend to be formed by simply binding the additional Li atom to the Al center of the smaller cluster ($Li_{n-1}Al$), (ii) for the larger clusters, n = 7 and 8, there is a competition between two growing modes, namely, binding Li directly to Al to form highly coordinated Al, and condensing Li on a (Li–Li–Li) surface to form a "tetrahedral unit". Our calculated results demonstrate that the neutral Li_5Al and the cation Li_6Al^+ are peculiarly stable with a high degree of aromaticity.

The stability pattern of these clusters, Li_nAl, can be interpreted successfully by using the phenomenological shell model (PSM). The clusters containing a "magic number" of valence electrons, such as Li_5Al and Li_6Al^+, are characterized by high thermodynamic stability. We hope that these

interesting Li systems will be experimentally detected and characterized in the near future.

Acknowledgements

We are indebted to the KULeuven Research Council (GOA, IDO and IUAP programs). TBT thanks the Arenberg Doctoral School of for a scholarship. MTN thanks the ICST for supporting his stays in Vietnam.

References

1 W. D. Knight, K. Clemenger, W. A. de Heer, W. A. Saunders, M. Y. Chou and M. L. Cohen, *Phys. Rev. Lett.*, 1984, **52**, 2141.
2 W. A. de Heer, *Rev. Mod. Phys.*, 1993, **65**, 611.
3 W. Bouwen, F. Vanhoutte, F. Despa, S. Bouckaert, S. Neukermans, L. T. Kuhn, H. Weidele, P. Lievens and R. E. Silverans, *Chem. Phys. Lett.*, 1999, **314**, 227.
4 K. Hoshino, K. Watanabe, Y. Konishi, T. Taguwa, A. Nakajima and K. Kaya, *Chem. Phys. Lett.*, 1994, **231**, 499.
5 M. Brack, *Rev. Mod. Phys.*, 1993, **65**, 677.
6 W. D. Knight, W. A. de Heer, K. Clemenger and W. A. Sauders, *Solid State Commun.*, 1985, **53**, 445.
7 M. M. Kappes, P. Radi, M. Schar and E. Schumacher, *Chem. Phys. Lett.*, 1985, **119**, 11.
8 C. Yeretzian, U. Rothlisberger and E. Schumacher, *Chem. Phys. Lett.*, 1995, **237**, 334.
9 E. Janssens, S. Neukermans and P. Lievens, *Curr. Opin. Solid. State Mater. Sci.*, 2004, **15**, 8.
10 C. Yeretzian, *J. Phys. Chem.*, 1995, **99**, 123.
11 H. P. Cheng, R. N. Barnett and U. Landman, *Phys. Rev. B: Condens. Matter*, 1993, **48**, 1820.
12 M. S. Lee, S. Gowtham, H. He, K. C. Lau, L. Pan and D. G. Kanhere, *Phys. Rev. B: Condens. Matter Mater. Phys.*, 2006, **74**, 245412.
13 V. Kumar, *Phys. Rev. B: Condens. Matter Mater. Phys.*, 1999, **60**, 2916.
14 J. Akola and M. Manninen, *Phys. Rev. B: Condens. Matter Mater. Phys.*, 2002, **65**, 245424.
15 S. Chacko and D. G. Kanhere, *Phys. Rev. A: At., Mol., Opt. Phys.*, 2004, **70**, 023204.
16 M. J. Frisch, G. W. Trucks, H. B. Schlegel, G. E. Scuseria, M. A. Robb, J. R. Cheeseman, J. A. Montgomery, Jr., T. Vreven, K. N. Kudin, J. C. Burant, J. M. Millam, S. S. Iyengar, J. Tomasi, V. Barone, B. Mennucci, M. Cossi, G. Scalmani, N. Rega, G. A. Petersson, H. Nakatsuji, M. Hada, M. Ehara, K. Toyota, R. Fukuda, J. Hasegawa, M. Ishida, T. Nakajima, Y. Honda, O. Kitao, H. Nakai, M. Klene, X. Li, J. E. Knox, H. P. Hratchian, J. B. Cross, V. Bakken, C. Adamo, J. Jaramillo, R. Gomperts, R. E. Stratmann, O. Yazyev, A. J. Austin, R. Cammi, C. Pomelli, J. Ochterski, P. Y. Ayala, K. Morokuma, G. A. Voth, P. Salvador, J. J. Dannenberg, V. G. Zakrzewski, S. Dapprich, A. D. Daniels, M. C. Strain, O. Farkas, D. K. Malick, A. D. Rabuck, K. Raghavachari, J. B. Foresman, J. V. Ortiz, Q. Cui, A. G. Baboul, S. Clifford, J. Cioslowski, B. B. Stefanov, G. Liu, A. Liashenko, P. Piskorz, I. Komaromi, R. L. Martin, D. J. Fox, T. Keith, M. A. Al-Laham, C. Y. Peng, A. Nanayakkara, M. Challacombe, P. M. W. Gill, B. G. Johnson, W. Chen, M. W. Wong, C. Gonzalez and J. A. Pople, *GAUSSIAN 03 (Revision C.02)*, Gaussian, Inc., Wallingford, CT, 2004.
17 H.-J. Werner, P. J. Knowles, R. Lindh, F. R. Manby, M. Schütz, P. Celani, T. Korona, A. Mitrushenkov, G. Rauhut, T. B. Adler, R. D. Amos, A. Bernhardsson, A. Berning, D. L. Cooper, M. J. O. Deegan, A. J. Dobbyn, F. Eckert, E. Goll, C. Hampel, G. Hetzer, T. Hrenar, G. Knizia, C. Köppl, Y. Liu, A. W. Lloyd, R. A. Mata, A. J. May, S. J. McNicholas, W. Meyer, M. E. Mura, A. Nicklass, P. Palmieri, K. Pflüger, R. Pitzer, M. Reiher, U. Schumann, H. Stoll, A. J. Stone, R. Tarroni, T. Thorsteinsson, M. Wang and A. Wolf, MOLPRO, version 2008.1, a package of *ab initio* programs.
18 R. G. Parr and W. Yang, *Density-Functional Theory of Atoms and Molecules*, Oxford University Press, Oxford, 1989.
19 A. D. Becke, *J. Chem. Phys.*, 1993, **98**, 5648.
20 J. P. Perdew, J. A. Chevary, S. H. Vosko, K. A. Jackson, M. R. Pederson, D. J. Singh and C. Fiolhais, *Phys. Rev. B: Condens. Matter*, 1992, **46**, 6671.
21 R. Krishnan, J. S. Binkley, R. Seeger and J. A. Pople, *J. Chem. Phys.*, 1980, **72**, 650.
22 J. Cizek, *Adv. Chem. Phys.*, 1969, **14**, 35.
23 P. J. Knowles, C. Hampel and H. J. Werner, *J. Chem. Phys.*, 1993, **99**, 5219.
24 K. Raghavachari, G. W. Trucks, J. A. Pople and M. Head-Gordon, *Chem. Phys. Lett.*, 1989, **157**, 479.
25 M. T. Nguyen, M. H. Matus, V. T. Ngan, D. J. Grant and D. A. Dixon, *J. Phys. Chem. A*, 2009, **113**, 4895.
26 T. B. Tai, D. J. Grant, M. T. Nguyen and D. A. Dixon, *J. Phys. Chem. A*, 2010, **114**, 994.
27 T. B. Tai, M. T. Nguyen and D. A. Dixon, *J. Phys. Chem. A*, 2010, **114**, 2893.
28 A. E. Reed, L. A. Curtiss and F. Weinhold, *Chem. Rev.*, 1988, **88**, 899.
29 J. P. Perdew, J. A. Chevary, S. H. Vosko, K. A. Jackson, M. R. Pederson, D. J. Singh and C. Fiolhais, *Phys. Rev. B: Condens. Matter*, 1992, **46**, 6671.
30 T. Clark, J. Chandrasekhar, G. W. Spitznagel and P. v. R. Schleyer, *J. Comput. Chem.*, 1983, **4**, 294.
31 M. Kohout, F. R. Wagner and Y. Grin, *Int. J. Quantum Chem.*, 2006, **106**, 1499.
32 F. R. Wagner, V. Bezuly, M. Kohout and Y. Grin, *Chem.–Eur. J.*, 2007, **13**, 5724.
33 M. Kohout, F. R. Wagner and Y. Grin, *Theor. Chem. Acc.*, 2002, **108**, 150.
34 M. Kohout, *DGrid-4.2*, Max-Planck Institut fur Chemische Physik und Fester Stoffe, Dresden, 2007.
35 L. Laaksonen, *J. Mol. Graphics*, 1992, **10**, 33.
36 K. A. Peterson, D. E. Woon and T. H. Dunning, *J. Chem. Phys.*, 1994, **100**, 7410.
37 Y. Li, D. Wu, Z. R. Li and C. C. Sun, *J. Comput. Chem.*, 2007, **28**, 1677..
38 V. T. Ngan, J. De Haeck, L. H. Thuy, G. Gopakumar, P. Lievens and M. T. Nguyen, *J. Phys. Chem. A*, 2009, **113**, 9080.
39 I. A. Boldyrev and L. S. Wang, *Chem. Rev.*, 2005, **105**, 3716.
40 A. N. Alexandrova and A. I. Boldyrev, *J. Chem. Theory Comput.*, 2005, **1**, 566.
41 (*a*) A. Datta, S. S. Mallajosyula and S. K. Pati, *Acc. Chem. Res.*, 2007, **40**, 213; (*b*) A. Datta and S. K. Pati, *J. Phys. Chem. A*, 2004, **108**, 9527; (*c*) A. Datta and S. K. Pati, *J. Am. Chem. Soc.*, 2005, **127**, 3496; (*d*) A. Datta and S. K. Pati, *J. Chem. Theory Comput.*, 2005, **1**, 824; (*e*) A. Datta and S. K. Pati, *Chem. Commun.*, 2005, 5032.
42 P. v. R. Schleyer, H. Jiao, N. J. R. V. E. Hommes, V. G. Malkin and O. L. Malkina, *J. Am. Chem. Soc.*, 1997, **119**, 12669.
43 K. Clemenger, *Phys. Rev. B: Condens. Matter*, 1985, **32**, 1359.

